Forensic Science International 363 (2024) 112200

Contents lists available at ScienceDirect

Forensic Science International

journal homepage: www.elsevier.com/locate/forsciint

An automated method for the generation of bloodstain pattern metrics from images of blood spatter patterns

Rosalyn Rough [a,b,*], Oliver Batchelor [b], Richard Green [b], Andrew Bainbridge-Smith [b]

[a] Institute of Environmental Science and Research Ltd (ESR), Christchurch Science Centre, P.O Box 29-181, Christchurch, New Zealand
[b] Department of Computer Science and Software Engineering, Faculty of Engineering, University of Canterbury, Private Bag, Christchurch 4800, New Zealand

ARTICLE INFO

Keywords:
Bloodstain pattern analysis
Automated
Quantitative
Metrics
Segmentation

ABSTRACT

An improved automated bloodstain pattern analysis method has been developed and validated, which utilises computer vision techniques to identify bloodstains on a plain background within a digital image. The method generates metrics relating to the individual stains as well as the overall pattern, including bloodstain pattern specific metrics such as the gamma angle, circularity, solidity, area of convergence, stain density and pattern linearity. This method provides an objective approach to the analysis of bloodstains and bloodstain patterns and can generate a wealth of quantitative data that is currently not obtainable using manual techniques or other image-based programs currently utilised in the discipline. This method will be useful to analysts and researchers investigating the application of quantitative methods to bloodstain pattern analysis.

1. Introduction

Bloodstain Pattern Analysis (BPA) is a discipline of forensic science that is concerned with the study of the size, shape and distribution of bloodstains deposited onto surfaces at bloodletting events, particularly crime scenes. With knowledge of the underlying principles of fluid mechanics, the physical characteristics of the stains can be analysed and used to assist with the reconstruction of the events that led to the bloodshed [1–3]. One of the key tasks in BPA is the classification of spatter patterns. Spatter patterns are groups of small circular and elliptical shaped bloodstains that have been formed as the result of some external force being applied to a source of liquid blood [4]. The current terminology of the different classes of spatter patterns in BPA relate to the mechanism of the force that caused them. Common types of spatter patterns present at crime scenes include impact (caused by an object striking liquid blood), swing cast-off (caused by blood released from a bloodstained object due to its swinging motion), and expirated (caused by the generation of droplets due to the force involved with the expulsion of blood from the mouth, nose or lungs) [4]. The application of these forces on the liquid blood results in its breakup into smaller droplets that travel through the air away from the blood source. When these predominately spherical droplets land onto nearby surfaces they collapse and spread on the target forming circular and elliptical shaped bloodstains.

BPA can be a valuable tool in investigations; however, the subjectivity of the discipline has been criticised [5,6] and disagreements between trained analysts have been documented in some high-profile cases [7,8]. A lack of empirical data and scientific foundations was cited as areas needed for improvement [5]. These criticisms have raised doubt over the reliability of the evidence that is often delivered in courtrooms. In response, reliability and black box studies have been undertaken to investigate the accuracy and reliability of bloodstain pattern classification. These studies have shown that some spatter patterns can have high error rates for classification [9–11]. This is not unsurprising as the mechanical process involved in the formation of spatter stains is the same regardless of the initial force applied. As a result, there are overlapping characteristics between different types of spatter patterns (for example, the range of stain sizes in a pattern) which can lead to ambiguity or misclassification. Studies have also shown some analysts are not always consistent with their classifications, classifying the same pattern differently when unknowingly presented with it a second time [12]. The inference being that there is a subjective approach to the classification process. There have been calls for more systematic guidelines within the discipline to assist with the classification task, but currently there is still no agreed criteria about what features are required to make a classification and the decision is left to the analyst based on their training, experience and level of confidence.

To reduce the subjectivity, quantitative methods have been

* Correspondence to: 27 Creyke Road, Ilam, Christchurch 8041, New Zealand.
E-mail address: rosalyn.rough@esr.cri.nz (R. Rough).

https://doi.org/10.1016/j.forsciint.2024.112200
Received 17 January 2024; Received in revised form 8 August 2024; Accepted 17 August 2024
Available online 20 August 2024

investigated to assist with BPA. Earlier research has applied image processing techniques to the analysis of digital images of bloodstains to automatically fit ellipses to the bloodstain shape and determine the impact angle and orientation angle from the minor and major axes. However, the described methodologies were applied to images of single bloodstains [13–15] or the procedure required input from the analyst to select the appropriate stains within a pattern [16,17]. More recently, researchers have utilised the quantitative techniques of Matlab [18–20] or ImageJ [21–23] to the analysis of digital images of bloodstain patterns. While both methods can easily extract the number of stains and give a measurement regarding their size, other BPA specific metrics are not available such as the directionality of the stain (represented numerically as the gamma angle), and the impact angle.

1.1. Gamma and impact angles

When a droplet lands on a target at an angle, the resultant stain is elliptical with the major (long) axis in alignment with the direction of travel. Furthermore, as the blood droplet collapses and spreads across the target a volume of the liquid can form a small wave that follows the direction of travel of the droplet. This wave can spill over from the contact line (the edge of the blood in the main parent stain) resulting in thin protrusions extending from the end of the parent elliptical stain [24]. Depending on the angle, droplet size and surface features, the protrusions can be single (referred as a tail), multiple (referred to as spines) and/or fully detach from the parent stain (see Fig. 1). The presence of these tails or spines on one side of an elliptical stain is considered a reliable indicator for the direction of travel along the major axis, and by combining the orientation angle with the direction, the gamma angle can be determined. For example, a stain on a 45-degree angle with a right direction will have a gamma angle of 45 degrees. However, if the same stain's directionality was left the gamma angle would be 225 degrees (see Fig. 2) [1].

Whilst the gamma angle can give information about the general direction a blood drop was travelling, the trajectory of the droplet can be estimated by including information on the angle the droplet impacted a target surface. It has been previously demonstrated that there is a relationship between the width to length ratio of an elliptical stain and the angle of impact (α) of the droplet to the target. Perpendicular impacts result in circular stains, more oblique angles result in more elongated elliptical stains. This relationship is shown in Eq.1 [25].

$$\alpha = \arcsin\frac{Width}{Length} \tag{1}$$

An accurate impact angle estimation relies on an accurate width and length measurement. One of the challenges faced by BPA analysts is accurately measuring the elliptical shape of the parent stain when the tails and spines lengthen the final stain. Analysts are trained to ignore these protrusions when estimating the length of the ellipse [26]. By combining the estimated impact and gamma angles a straight-line trajectory of the droplet can be determined. It is noted that the other influencing forces such as gravity and drag are ignored during this estimation.

Determining these angles for various stains can assist with grouping stains together as part of the same pattern/event and also can be used to limit the positions of the blood source within a geometric space and therefore assist with reconstruction of events at a scene. Most analysis at crime scenes is still undertaken manually and each spatter pattern can contain hundreds to thousands of stains. So, whilst the gamma and impact angles are considered important features there is currently neither the time nor the resources to collect data on every individual stain.

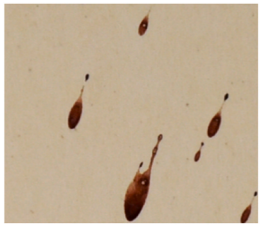

Fig. 1. Stains with tails and spines indicating right and upward directionality.

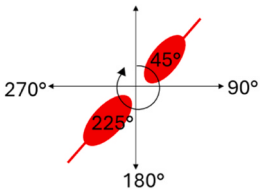

Fig. 2. Schematic representation of bloodstain gamma angles.

In 2017 image processing techniques were applied to develop a methodology that can automatically extract bloodstain pattern features from digital images [18]. Using Matlab R2015B the digital image of an impact pattern was imported, the background subtracted, and the objects of interest (stains) segmented using the Triangle thresholding algorithm. To overcome the challenge of fitting accurate ellipses to stains with spines, the researchers applied erosion and dilation morphological operations to remove small protrusions and background noise. Stains greater than 10 pixels in both the original binarised image and the eroded/dilated image were then mapped, linked and relevant measurements computed using Matlab regionprops [18]. In this research the direction of the stains was determined by locating the centroid of the ellipse from the eroded/dilated image within the bounding box of the original stain. This along with the orientation angle was used to calculate the gamma angle. Other BPA specific features were also computed. These included shape features of the individual stains (tail to body ratio, width to length ratio, area of stain to area of convex hull ratio (regularity measure), ratio of perimeter of inscribed circle to perimeter of stain, stain size and stain intensity. Five pattern features were also calculated: overall directionality, convergence, linearity, circularity of pattern, stain density.

Subsequently this methodology was applied to a limited number of laboratory generated impact and cast-off patterns [27] and the results analysed. A combination of five of the above-described features were found to be optimal for distinguishing between these two classes of patterns. Although demonstrating a promising approach to the application of an automated system to the analysis of spatter patterns, Matlab licences are expensive and not all researchers and BPA analysts have easy access to this platform. Furthermore, the fixed thresholding values did not work well when the methodology was applied to further laboratory generated spatter patterns created in our research facilities and the system was slow to analyse patterns with thousands of stains [28].

We present an Automated Bloodstain Pattern Analysis method (ABPA method) that improves on the previous methodology described [18], increasing the detection of the small stains present in the patterns, and computing more suitable BPA specific metrics that have been developed based on the results of prior research [27,28] and on an understanding of the fluid mechanics underpinning the formation of blood spatter patterns. This application has been implemented in Python, importing modules including numpy, matplotlib, and Open CV for easy implementation of image segmentation and analysis. Python has the benefit of being a free open-source language that is readily available to researchers, academics and analysts, making the method more accessible than Matlab.

2. Pattern images

During the development of the proposed ABPA method high-resolution images of impact, cast-off and expirated bloodstain patterns

were used. The patterns were laboratory generated using porcine blood, and a food safe blood substitute (42.5 % w/v liquid honey, 20 % w/v water-based dye, 10 % w/v pasteurised egg white, and 27.5 % w/v deionised water). Surface tension and viscosity were not measured. The patterns were created on paper targets, with a wide range of variables including volume of blood, variations of force applied and various objects or expirated mechanisms used. The resulting patterns ranged from singular stains to up to thousands of stains depending on the variables used. A Canon EOS 5Ds with a 24–70 mm lens was used to photograph the bloodstain patterns. For each photo the same settings were used: 8688 ×4888 pixels resolution, 70 mm zoom, diaphragm opening of f5.6, shutter speed of 1/125 s and automatic ISO and focus, resulting in all images having a resolution of 7.9 pixels per mm. Multiple images were taken for each pattern to capture all the stains and these were stitched together using photo stitching software (PTGui version V10.0.17). In order to stitch these images together, pins or stickers were placed in the images to act as reference points. Therefore, in addition to the bloodstains, most images had markers as well as rulers around the edge to show the scale.

3. Development of automated bloodstain pattern analysis method

The methodology presented in this paper takes a digital image of a bloodstain pattern, identifies the individual bloodstains, calculates metrics for each individual stain and metrics for the overall pattern. Improvements to both the segmentation of the stains and the methods for calculating bloodstain metrics have been implemented.

3.1. Cropping of images

To segment the bloodstains, it was assumed that the image had a lighter background to the bloodstains and no other objects were in the image apart from circular stickers used for stitching. This is a reasonable assumption for research purposes. Any rulers present in the images were therefore required to be removed. An automatic cropping function previously developed [28], was incorporated into the methodology to achieve this. However, this method assumes there are four rulers, on all four edges, so for images with less than four rulers the rulers were required to be manually cropped.

3.2. Stain segmentation

As part of the cropping process the image was first blurred with a Gaussian blur and converted to grey scale. A novel approach to the detection of the bloodstains in the images was then developed. Rather than using Triangle or Otsu thresholding which have been used in prior research [14,18,28] and which rely on the entire image having a consistent histogram, the grey scale image was converted to binary with adaptive thresholding. Adaptive thresholding calculates the threshold value for smaller regions of the image determined by a block size which leads to different threshold values for regions which have changes in lighting, reducing the effect of shadows and noise [29]. The adaptive thresholding method applied was based on the Gaussian mean value of a block in the image then a constant offset parameter was applied. The block size was set at 99 pixels for all images. The binary image was produced by setting all pixels with values below the threshold to black and all pixels with values above the threshold to white resulting in white stains on a black background.

An opening morphology operation (erosion followed by dilation) to reduce noise and remove some protrusions that are not significant, was then performed on the binary image as described in [28]. Circular stickers added to assist with image stitching were removed by incorporating the Hough circle transform algorithm [30] as detailed in [28]. Finally, each stain or polygon was found by finding the contours of the image using the Suki border algorithm [31]. Stain less than 5 pixels were not counted due to the uncertainty of them being true stains versus background noise.

3.3. Bloodstain metrics

Ten different outputs were developed and computed for each individual stain in the image. These, along with the four developed pattern metrics are summarised in Table 1.

Each stain was designated an identification number and the X and Y positions for the centroid were computed. The area of the bloodstain was simply a count of all the pixels in the stain boundary. The inputted scale value (pixels per mm) was used to covert this value to area in mm^2. The pixel count was retained as this was found to be a useful metric when sorting and applying thresholds to the outputted data. The intensity was measured by the normalised average grey scale value of the pixels in the stain and was used as a measure of lightness for the stains. The solidity (a measure of boundary smoothness or regularity) of the stains was determined by the ratio of the area of the stain to the area of the convex hull of the stain. Smooth edged stains with no protrusions will have a solidity value close to 1.

3.4. Ellipse fitting

The remaining five bloodstain metrics required the fitting of an ellipse for calculation. As discussed, any tails or protrusions will falsely elongate the length of any fitted ellipse, and therefore these need to be removed prior to any ellipse fitting. Rather than using an erosion and dilation operation that has been used in prior research, a novel solution to the task of removing the tails was developed. This involved identifying the concave points along the stain boundary, then starting from the furthest point away from the centroid, the algorithm stepped around the stain in both directions measuring the distance between the two points. When the ratio of this distance to the maximum width or height of the bloodstain was greater than 0.3 and one of these points was a concave point, the end of the tail is identified. All points between these two points were removed so the tail was removed. The ellipse was then fitted to the resulting polygon using the least squares method [32].

The size of the width and length of the ellipse was then measured. The shape of the ellipse was represented in the circularity metric, calculated as a ratio of the ellipse width and length. A stain with a circularity measure of 1 is circular, a stain with a circularity close to 0 is very elongated.

The orientation angle of the stain was measured clockwise from vertical from the centre of the bloodstain with the range of between 0 and 179 degrees. As discussed, to determine the gamma angle the horizontal direction of the stain is also required. To determine the horizontal direction of each stain a convex hull of the contour line was applied and the furthest point on the contour from the centre of the stain was determined to be the end of the tail. Differences in the X co-

Table 1
Summary of bloodstain and pattern metrics computed by the ABPA method.

Property	Feature	Stain/pattern
Position	X,Y co-ordinates	Stain polygon
Size	Size (pixels)	Stain polygon
Size	Size mm^2	Stain polygon
Lightness	Intensity	Stain polygon
Shape	Solidity	Stain polygon
Shape	Ellipse width and height	Fitted stain ellipse
Shape	Circularity	Fitted stain ellipse
Orientation	Orientation angle	Fitted stain ellipse
Shape	Direction	Fitted stain ellipse
Orientation	Gamma angle	Fitted stain ellipse
Shape	Linearity	Pattern
Distribution of stains	Density of stain number	Pattern
Proportion of staining	Density of stain area	Pattern
Shape	Convergence	Pattern

ordinates between the centre of the stain and the furthest point away were calculated with negative values indicating a left direction. For stains with left directionality, the gamma angle equates to the angle of the stain plus 180 degrees.

For stains that are not particularly elliptical, determining a reliable directionality is difficult, if not impossible as tails and protrusions are usually not formed, and the leading edge of the stain cannot be identified. Therefore, a threshold ratio of 0.86 was set (which equates to approximately 60-degree angle of impact) as stains made at impact angles above this do not usually display tails or protrusions. Thus, directionality was not calculated for stains which had a width to length ratio greater than 0.86 to ensure only reliable directionality measurements were calculated.

3.5. Pattern metrics

Three pattern metrics were selected for computation: linearity, convergence and distribution of stains. The linearity was chosen as a mathematical representative of how linear or not a pattern was. It is expected that patterns such as cast-off will have a more linear shape than radiating patterns from a stationary source of blood such as an impact, and therefore may be a useful measurement for discrimination. The linearity was calculated by plotting all the stain centroids and fitting them to a two-degree polynomial curve using numpy's "polyfit" function with an output graph [33].

A small area of convergence in a pattern indicates that the stains originated from a small area, suggesting a stationary source of blood, and is expected to be observed in impact patterns (and expirated patterns). To identify the area of convergence, a line following the major axis of the ellipse was extended back to the edge of the image for all stains with fitted ellipses. A sliding window algorithm over these line segments found all of the intersections. A density matrix was calculated with the Gaussian kernel density estimator described in [34] with 25 bins and then plotted using a heat map. A box was fitted around the area that contained 60 % of the intersections and the co-ordinates of this box were computed.

A convex hull was applied to the entire pattern to calculate the total area of the pattern. The distribution of the stains was then calculated in two different ways, the first was simply the total number of stains divided by the pattern area, and secondly, the total area of the stains divided by the pattern area which gave a proportion of the pattern that was stains.

3.6. User interface

A user interface was developed to increase usability of the application. This enables the user to select which annotations to display, which pattern metrics to compute, and which results to export.

The user interface also enables the analyst to zoom in on a selected stain when the row representing that stain is selected, creating a link between the data and the selected stain. This allows the results to be checked against the physical characteristics of the stain to ensure accuracy. Batch processing was also made available so an entire folder of images can be processed with no further user interaction.

3.7. Outputs

A digital image of a spatter pattern is used as the input along with the known resolution of the image (in pixels per mm). The method delivers the individual bloodstain metrics as a comma separated file (containing one line for each stain and columns for each metric) and an annotated image with selected features displayed. The overall pattern metrics are delivered as a further comma separated file, and three graphs are produced to display convergence, linearity and distribution of the stains. The co-ordinates for all boundary pixels for each stains are also produced in a separate comma separated file, with each row representing

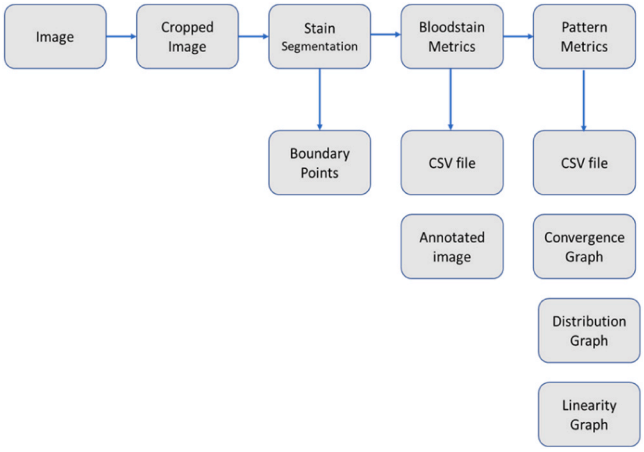

Fig. 4. Workflow of developed ABPA method.

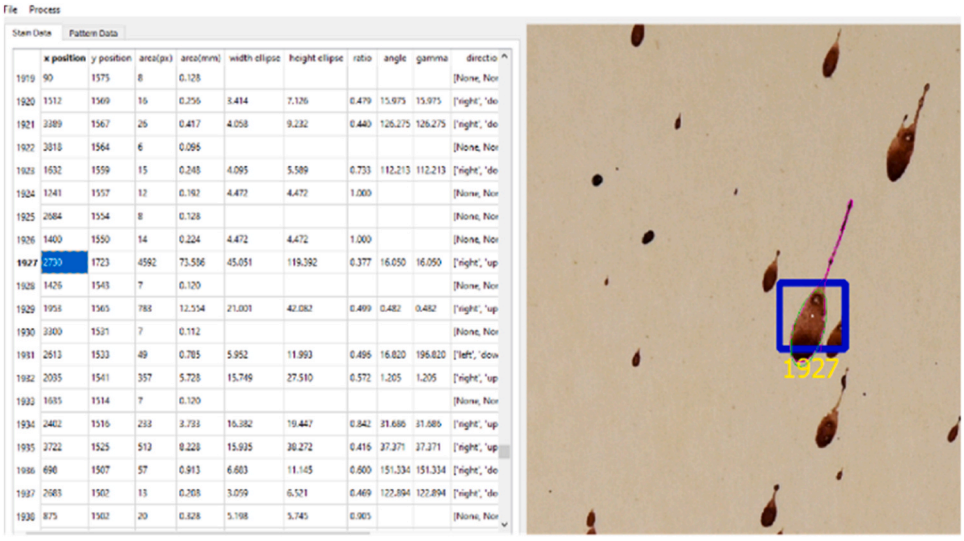

Fig. 3. Screenshot showing user interface with stain 1927 selected for an impact pattern. The stain boundary is annotated in pink and the fitted ellipse annotated in green. Metrics are listed on the left.

the co-ordinates for each stain. This workflow is represented in Fig. 4.

4. Results

The proposed ABPA method was applied to 132 cast-off, 208 impact and 132 expirated patterns that were generated in the laboratory as previously described in Section 2, and the outputted results scrutinised by a trained BPA analyst.

4.1. Segmentation

All bloodstains that were able to be visually identified by the analyst in the outputted image file were annotated by the method. This included very small stains less than 0.5 mm in diameter. However some false positives were detected, such as staple holes and shadows at the edge of some images. Any markings from rulers not completely cropped out would also be identified as stains as would any non-circular pins present in the image.

4.2. Comparison with ImageJ

Three patterns from each class (expirated, cast-off and impact) representing a variety of different stains numbers, sizes and intensities were analysed with both ImageJ (using the auto thresholding function) and the proposed ABPA method and the number of stains identified with each were compared. As ImageJ did not have a minimum stain size, a count of stains greater than 4 pixels was calculated for the ImageJ results for comparisons which are noted in Table 2. It is noted that there was a big difference between stain numbers for impact pattern 14 and expirated pattern 87 between the two methods, with the proposed ABPA method detecting more stains than ImageJ. When qualitatively comparing the binary output of ImageJ with the pattern overlay output of the ABPA method it is apparent that ImageJ is not detecting all of the stains in the image.

For impact 14 a larger volume of blood was used resulting in larger and darker stains within the pattern. As a result, the thresholding for ImageJ is not detecting the smaller and fainter stains (Fig. 6). Likewise, for the expirated pattern 87, due to the blood substitute being a paler colour and then further diluted with saliva during the spitting action to create the pattern, many of the stains are pale and these are not all being detected by ImageJ.

The propsed ABPA method also coped better with shadows and uneven lighting. For expirated pattern 53 (Fig. 7) the shadowing on the lower portion of the image was counted as stains in ImageJ, and was largely ignored with the proposed ABPA method. This is represented in the total stain count of 8383 with ImageJ, reducing by nearly half to 4773 when stains less than 5 pixels are removed. This is much more comparable to the 4613 stains identified with the ABPA method. This result also validates our decision to limit noise by having a minimum stain size of 5 pixels for the proposed ABPA method.

Table 2
Comparison of number of stains identified.

Pattern ID	Class	Total stains ImageJ	>4 pixels ImageJ	Total stains ABPA
16c	castoff	110	98	103
103	castoff	12	11	11
133	castoff	344	233	281
14	impact	2747	1769	3315
13	impact	442	277	335
77	impact	1144	1090	1133
87	expirated	241	176	575
9	expirated	11006	7843	7780
53	expirated	8383	4773	4613

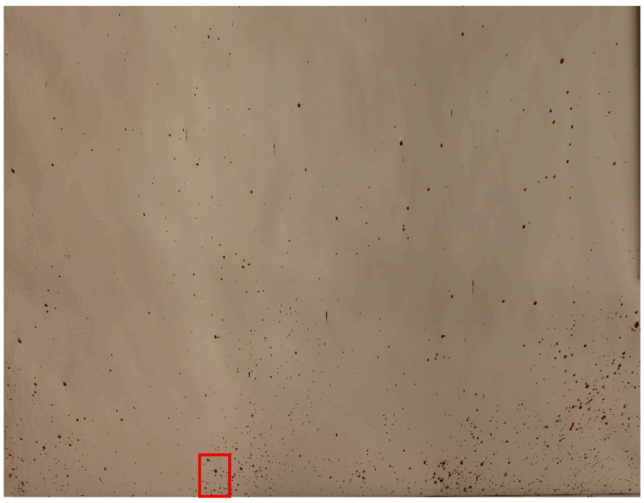

Fig. 5. Lower half of impact pattern 14 (original cropped image), with small area slecetd by red box.

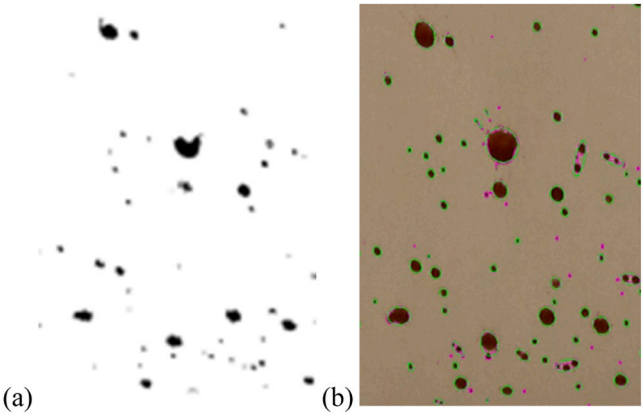

Fig. 6. Close up of area outlined by the red box in Fig. 5 for (a) ImageJ binarised output and (b) annotated image of ABPA method. Note less stains have been identified in (a) (ImageJ) compared to (b) (ABPA method).

4.3. Comparison with Matlab method

The impact pattern analysed with the Matlab method in [18] was made available to the authors and was analysed with our developed ABPA method. The proposed ABPA method detected 1623 stains of 10 pixels or greater, much more than the 420 labelled elements identified in the original research paper. The improved segmentation process is likely to account for the increase in stains detected, as well as the ability of the proposed ABPA method to count and measure all stains not just those with fitted ellipses.

Overall, the results indicate that the proposed ABPA method has a reliable and sensitive stain segmentation method that copes well with shadows and uneven lighting, and different intensity stains and is an improvement on both the automated thresholding of ImageJ and the previous Matlab developed methodology.

4.4. Ellipse fitting and bloodstain metrics

Ellipses were fitted well to well-formed elliptical and spherical stains. However, as the method attempted to fit ellipses to all stains there were times when very large ellipses were overlayed onto stains, particularly for ones that had flowed, or were overlapping with other stains. Examples are shown in Fig. 8. Currently the only solution to remove these is to identify these stains using the user interface and

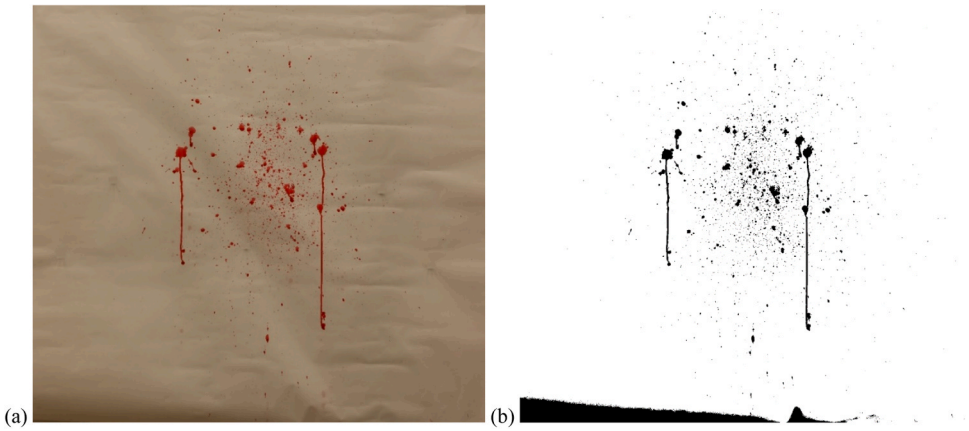

Fig. 7. (a) Expirated pattern 53 original cropped image (b) binarised ImageJ output. Note shadowing at the lower left of image has been detected by ImageJ.

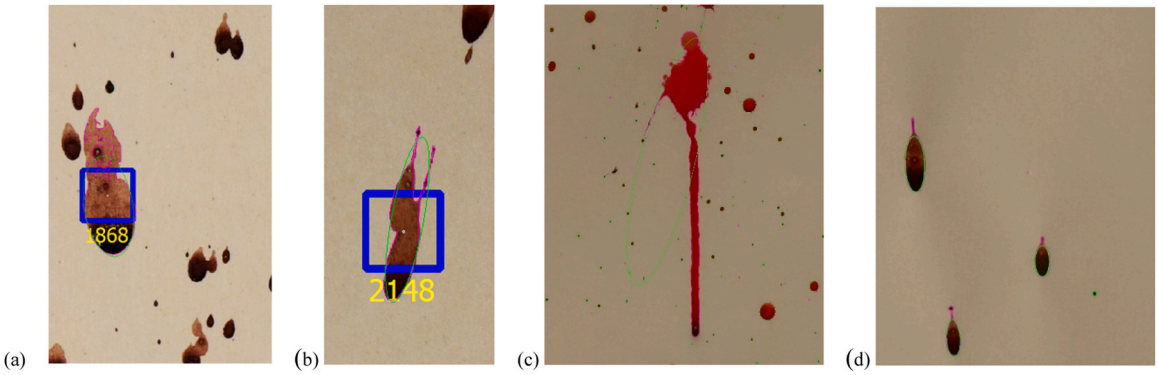

Fig. 8. showing examples of fitted ellipses to compound stains (a,b), flows (c) and well-formed stains (d). The boundary of the stain is marked in pink, with the fitted ellipse in green. For (d), the ellipses have fitted well to the main portion of the stain and the tails have been ignored as intended.

remove their data from the file once it has been saved. Some stains did not have enough points around their contour to fit an ellipse. This resulted in empty values for the width, height, direction, angle and gamma angle, however other metrics such as area and position were still able to be measured. The bloodstain metrics for the 11 stains in cast-off pattern 103 are displayed in Table 3.

4.5. Pattern metrics

The pattern metric outputs for the three different patterns (impact 14, cast-off 103 and expirated 9) are displayed in Table 4.

For the linearity, the centroids of the stains were plotted and a 2-degree polynomial was fitted to the points (see Fig. 10). The measure of how well the points fitted to the curve were represented by the calculated R^2 value. The R^2 values for both the impact and expirated patterns were very low indicating the centroid points did not fit well to a curved line. The R^2 value for the cast-off pattern was higher which is expected as this pattern type is more linear than the other two which are radiating patterns. As not all cast-off patterns produced stains in a strongly linear distribution a large range of R^2 values (ranging from 0.1 to 0.99) were noted for these types of patterns.

Likewise, both density measurements (ratio of the stain number to pattern area and ratio of stain area to pattern area) is lowest for cast-off which is expected as this pattern has a smaller number of stains. The

Table 3
Example of bloodstain metrics output (from cast-off pattern 103).

Id	Position X	Position Y	Area px	Area mm	Width ellipse	Height ellipse	Angle	Gamma	Direction	Solidity	Circularity	Intensity
0	2422	8343	44	0.705	5.389	11.152	178.467	178.467	('right', 'down')	0.936	0.483	0.427
1	370	6949	6	0.104						0.929		0.434
2	943	6556	86	1.378	6.347	21.639	177.972	177.972	('right', 'down')	0.8	0.293	0.259
3	943	6487	523	8.388	11.456	51.01	0.389	0.389	('right', 'up')	0.802	0.225	0.178
4	1091	4899	128	2.059	6.7	31.227	3.172	183.172	('left', 'down')	0.843	0.215	0.234
5	30	4851	101	1.626	10.559	12.652	80.98	260.98	('left', 'down')	0.923	0.835	0.324
6	1094	4782	1565	25.076	19.693	129.393	1.52	181.52	('left', 'down')	0.765	0.152	0.16
7	4	2586	18	0.296	4	7	90	90	?	0.725	0.571	0.366
8	380	2314	83	1.33	6.737	16.687	5.165	5.165	('right', 'up')	0.912	0.404	0.205
9	1053	2000	366	5.872	12.379	36.851	178.874	178.874	('right', 'down')	0.868	0.336	0.144
10	1824	1981	431	6.906	13.886	40.185	177.683	357.683	('left', 'up')	0.876	0.346	0.125

Table 4
Pattern metrics for 3 different patterns.

	Impact 14	Cast-off 103	Expirated 9
Linearity - Polyline fit	2.82e−05 x^2–0.194 x + 1.122e+04	0.0006217 x^2–0.5498 x + 4378	3.512e−05 x^2–0.2742 x + 3425
R^2	0.0022	0.1084	0.0017
Distribution - ratio stain number to convex hull area	3.87E−05	1.01E−06	1.92E−04
ratio stain area to convex hull area	4.49E−03	3.08E−04	1.25E−02
Convergence - point of highest density	(3124.0, 12098.0)	(1085.7, 4797.2)	(3564.0, 2915.0)
box of %60 of intersections	lower left (x,y): (2556.1,11572.1) Width: 3691.9 Height: 1051.9	lower left (x,y): (771.6,1884.5) Width: 628.2 Height: 3883.6	lower left (x,y): (2970.0,1855.0) Width: 594.0 Height: 1590.0

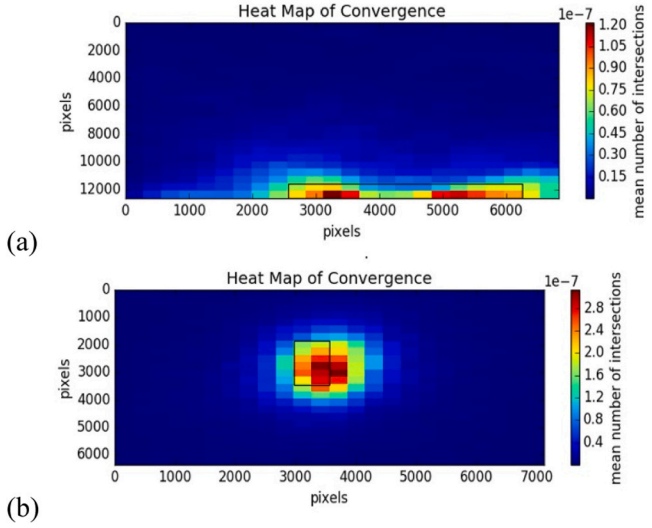

Fig. 9. Heat map of convergence for (a) Impact pattern 14 and (b) Expirated pattern 9.

expirated pattern has the highest density measurement, which again is consistent with this pattern having the largest number of stains. However, these density measurements appear to be lower than expected for expirated and impact and this is likely to be due to the area of the convex hull of the pattern being measured larger than it truly is due to false positives near the edges of the target. As such it is likely that the density measurements for expirated and impact in particular are lower than the true values.

The convergence box calculated for cast-off 103 was much larger than for the other two patterns reflecting the fact that cast-off patterns are not expected to have an area of convergence because the source of the blood is not stationary. Fig. 9 shows the convergence heat maps for impact 14 and expirated 9, and the centre of these heat maps accurately represent the differing positions of the blood source when these patterns were created (close to the bottom of the target for impact and centrally for expirated). For some cast-off patterns with limited stain numbers the convergence was unable to be computed as there were no intersecting directional lines.

The convergence metric was the longest pattern metric to calculate particularly for patterns with many stains as this created many intersections between the different stains directional paths which had to be identified and counted.

5. Conclusions

Our main goal was to increase the objectivity of BPA by developing a method that could be used to extract quantitative data, including BPA specific metrics, quickly and reliably from digital images of spatter bloodstain patterns.

The developed ABPA method described in this paper is an improvement on methodologies described in prior research relating to quantitative BPA. We have demonstrated that the proposed ABPA method has a reliable and sensitive stain segmentation methodology that copes well with shadows and uneven lighting, as well as different stain intensities, and is an improvement on both ImageJ and the previously reported Matlab developed method [18]. More stains and less background noise and/or false positives were identified with the proposed ABPA method compared to the previously described methodologies. However, some false positives such as staple holes or marks from rulers were still identified as stains.

With regards to the BPA specific metrics, a novel approach to ignoring tails and fitting ellipses was established resulting in accurate ellipse fitting and therefore accurate impact angle calculations for the elliptical stains. A reliable approach to determining the location of the tail or spines on the stains and therefore their directionality was also developed. Using the directionality and the orientation angle, the BPA specific gamma angle was calculated for all stains with a circularity below 0.86. However, there were some challenges with irregular shaped stains (such as compound stains and flows) and the method struggled to fit accurate ellipses to these stains. Implementing a methodology to identify overlapping ellipses would improve the outputs of the ABPA

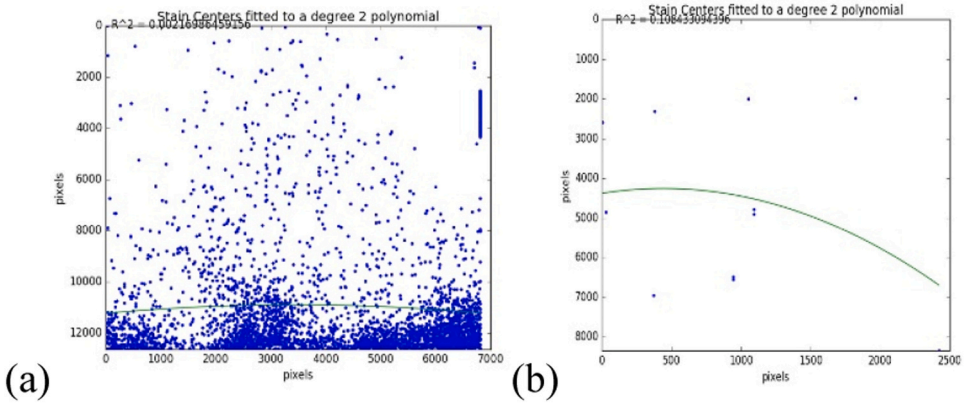

Fig. 10. Linearity map for (a) Impact pattern 14 and (b) Cast-off pattern 103.

method in the future. Improvements could also be made to the density calculations which currently seem overinfluenced by outliers in a pattern, which greatly increase the overall pattern size, thus reducing the density.

A user interface was also developed which linked stain data to the identified stains in the image, allowing for individual stains to be identified within the image and scrutinised against their calculated metrics. This interface can be used to identify those false positives and irregular shaped stains with poorly fitted ellipses. Their metrics can then be manually removed from the pattern outputs.

The method coped well with all of the laboratory generated pattern images it was applied to (132 cast-off, 208 impact and 132 expirated patterns). These images range in overall size, shape and orientation as reflected by the differing target sizes used for the different pattern types. It was determined from the ABPA method that the number of stains present in these patterns ranged from 1 to over 9500 stains. Generally, patterns were processed within a few minutes, with patterns containing thousands of stains taking longer to calculate the convergence metric due to the sheer volume of intersections of the directional lines of the stains.

Having demonstrated that the developed ABPA method can cope with a range of pattern types and produces accurate and reliable stain and pattern metrics it is hoped further researchers will utilise the method. By using Python and open source computer vision libraries no licenses are required to run the method which is also seen as a benefit as it improves accessibility to other analysts and researchers. It is envisioned that the data generated from the dataset of the three spatter pattern classes used during this validation process will now be statistically analysed, with the intention of potentially discovering measurable stain and pattern features that will be diagnostic for classifying different pattern classes.

CRediT authorship contribution statement

Richard Green: Writing – review & editing, Supervision. **Andrew Bainbridge-Smith:** Writing – review & editing, Supervision. **Rosalyn Marie Rough:** Writing – original draft, Validation, Methodology, Conceptualization. **Oliver Batchelor:** Software, Methodology.

Declaration of Competing Interest

The authors declare that they have no known competing financial interests or personal relationships that could have appeared to influence the work reported in this paper.

Acknowledgements

The authors gratefully acknowledge Dr Ravishka Arthur for access to her implementation and impact pattern for validation. The authors would also like to acknowledge the contribution of the late Dr Michael Taylor for supporting this research and offering valuable advice. This work was supported by the Institute of Environmental Science and Research (ESR), New Zealand. This work was also carried out as part of doctoral research through the University of Canterbury.

References

[1] T. Bevel, R.M. Gardner, Bloodstain pattern analysis with an introduction to crime scene reconstruction, CRC Press, Boca Raton, FL, USA, 2008.
[2] S. James, P. Kish, P. Sutton, Principles of bloodstain pattern analysis: theory and practice, taylor and francis group, Florida (2005).
[3] D. Attinger, C. Moore, A. Donaldson, A. Jafari, H.A. Stone, Fluid dynamics topics in bloodstain pattern analysis: comparative review and research opportunities, Forensic Sci. Int. 231 (2013) 375–396.
[4] ASB Technical Report 033, Terms and Definitions in Bloodstain Pattern Analysis, First Edition, 2019.
[5] National Research Council, Strengthening Forensic Science in the United States: A Path Forward, ed. C.o.A.a.T.S.N.R.C. Commitee on Identifying the Needs of the Forensic Science Community. 2009, Washington, DC: The National Academy of Sciences. (b) Strengthening Forensic Science in the United States: A Path Forward, Committee on Identifying the Needs of the Forensic Sciences Community, National Research Council, The National Academies Press, Washington, DC. 2009. https://doi.org/10.17226/12589.
[6] Collof, P. Blood Will Tell, Propublica, 2018, ⟨https://www.propublica.org/article/bloodstain-pattern-analysis-jury-wrongful-conviction-acquitted-exonerated⟩.
[7] Indiana v. David Camm, 812 N.E.2d 1127 (Ind. App., 2004).
[8] People v. McWhorter, 47 Cal. 4th 318, 330–332 (2009).
[9] M.C. Taylor, T.L. Laber, P.E. Kish, G. Owens, N.K. Osborne, The reliability of pattern classification in bloodstain pattern analysis, part 1: bloodstain patterns on rigid non-absorbent surfaces, J. Forensic Sci. 61 (4) (2016) 922–927.
[10] M.C. Taylor, T.L. Laber, P.E. Kish, G. Owens, N.K. Osborne, The reliability of pattern classification in bloodstain pattern analysis—part 2: bloodstain patterns on fabric surfaces, J. Forensic Sci. 61 (6) (2016) 1461–1466.
[11] R.A. Hicklin, K.R. Winer, P.E. Kish, C.L. Parks, W. Chapman, K. Dunagan, T. A. Busey, Accuracy and reproducibility of conclusions by forensic bloodstain pattern analysts, Forensic Sci. Int. 325 (2021) 110856.
[12] Ristenpart, W., Tulleners, F., Siu, S., Saifi, J., and Springer, F. (2013). Quantitative analysis of high velocity bloodstain patterns. NCJ Number 241744.
[13] P. Joris, W. Develter, E. Jenar, P. Suetens, D. Vandermeulen, W. Van de Voorde, P. Claes, Calculation of bloodstain impact angles using an active bloodstain shape model, J. Forensic Radiol. Imaging 2 (4) (2014) 188–198.
[14] K. Boonkhong, M. Karnjanadecha, P. Aiyarak, Impact angle analysis of bloodstains using a simple image processing technique, Sonklanakarin J. Sci. Technol. 32 (2) (2010) 169.
[15] N.J. Shoumy, P. Ehkan, S.N. Yaakob, M.S. Ali, S. Khatun, Feature extraction for neural network pattern recognition for bloodstain analysis, Int. J. Appl. Eng. Res. 11 (15) (2016) 8583–8589.
[16] P. Joris, W. Develter, E. Jenar, P. Suetens, D. Vandermeulen, W. Van de Voorde, P. Claes, HemoVision: an automated and virtual approach to bloodstain pattern analysis, Forensic Sci. Int. 251 (2015) 116–123.
[17] A.R. Shen, G.J. Brostow, R. Cipolla, Toward automatic blood spatter analysis in crime scenes, IET Conf. Crime. Secur. (2006) 378–383.
[18] R.M. Arthur, P.J. Humburg, J. Hoogenboom, M. Baiker, M.C. Taylor, K.G. de Bruin, An image-processing methodology for extracting bloodstain pattern features, Forensic Sci. Int. 277 (2017) 122–132.
[19] S. Siu, J. Pender, F. Springer, F. Tulleners, W. Ristenpart, Quantitative differentiation of bloodstain patterns resulting from gunshot and blunt force impacts, J. Forensic Sci. 62 (5) (2017) 1166–1179.
[20] Y. Liu, D. Attinger, K. De Brabanter, Automatic classification of bloodstain patterns caused by gunshot and blunt impact at various distances, J. Forensic Sci. 65 (3) (2020) 729–743.
[21] T. Stotesbury, M. Illes, A. Vreugdenhil, Investigation of physical effects of Acid Yellow 7® enhancement on dark and non-porous surfaces in impact pattern area of origin estimation, Can. Soc. Forensic Sci. J. 45 (1) (2012) 22–35.
[22] T.C. De Castro, D.J. Carr, M.C. Taylor, J.A. Kieser, W. Duncan, Drip bloodstain appearance on inclined apparel fabrics: Effect of prior-laundering, fibre content and fabric structure, Forensic Sci. Int. 266 (2016) 488–501.
[23] K. Boos, A. Orr, M. Illes, T. Stotesbury, Characterizing drip patterns in bloodstain pattern analysis: An investigation of the influence of droplet impact velocity and number of droplets on static pattern features, Forensic Sci. Int. 301 (2019) 55–66.
[24] P.A. Pizzola, S. Roth, P.R. De Forest, Blood droplet dynamics—I, J. Forensic Sci. 31 (1) (1986) 36–49.
[25] V. Balthazard, R. Piedelievre, H. Desoille, L. DeRobert, Study of projected drops of blood, Ann. Med. Leg. Criminol. Police Sci. Toxicol. 19 (1939) 265–323.
[26] M. Reynolds, M.A. Raymond, New bloodstain measurement process using Microsoft Office Excel 2003 autoshapes, J. Forensic Identif. 58 (4) (2008) 453.
[27] R.M. Arthur, J. Hoogenboom, M. Baiker, M.C. Taylor, K.G. De Bruin, An automated approach to the classification of impact spatter and cast-off bloodstain patterns, Forensic Sci. Int. 289 (2018) 310–319.
[28] Barnaby, C., and Green, R. (2018, November). Blood Stain Segmentation. In 2018 International Conference on Image and Vision Computing New Zealand (IVCNZ) (pp. 1-9). IEEE.
[29] ⟨https://docs.opencv.org/4.x/d7/d4d/tutorial_py_thresholding.html⟩.
[30] D.H. Ballard, Generalizing the hough transform to detect arbitrary shapes, Pattern Recognit. 13 (2) (1981) 111–122.
[31] S. Suzuki, Topological structural analysis of digitized binary images by border following, Comput. Vis., Graph., Image Process. 30 (1) (1985) 32–46.
[32] A. Fitzgibbon, M. Pilu, R.B. Fisher, Direct least square fitting of ellipses, IEEE Trans. Pattern Anal. Mach. Intell. 21 (5) (1999) 476–480.
[33] Accessed 19 Oct 2022 Numpy API References ⟨https://numpy.org/doc/stable/reference/generated/numpy.polyfit.html⟩.
[34] T. Ledl, Kernel density estimation: theory and application in discriminant analysis, Austrian J. Stat. 33 (3) (2004) 267–279.